Sensing and Bio-Sensing Research 23 (2019) 100262

Contents lists available at ScienceDirect

Sensing and Bio-Sensing Research

journal homepage: www.elsevier.com/locate/sbsr

Elemental Cu doped Co_3O_4 thin film for highly sensitive non-enzymatic glucose detection

Micaela Harry[a], Mahabubur Chowdhury[a,*], Franscious Cummings[b], Christopher J. Arendse[c]

[a] Department of Chemical Engineering, Cape Peninsula University of Technology, Cape Town 8000, South Africa
[b] Electron Microscope Unit, University of the Western Cape, Bellville 7535, South Africa
[c] Department of Physics and Astronomy, University of the Western Cape, Bellville 7535, South Africa

ARTICLE INFO

Keywords:
Co_3O_4
Non-enzymatic sensor
Glucose sensor
Thin film

ABSTRACT

We report on the non-enzymatic glucose sensing ability of elemental Cu doped Co_3O_4 thin film deposited on FTO in this study. A facile chemical solution method was used to substitute elemental Cu into the Co_3O_4 host lattice. The morphology of the electrode was characterized by XRD, SEM, HRTEM, SAED and EELS. The as prepared thin film exhibited very high sensitivity of 1850 $\mu Acm^{-2} mM^{-1}$, and linear range up to 7.6 mM. The sensor showed a limit of detection of 153 nM at a signal to noise ratio of 3. The developed sensor was used successfully to measure glucose level in human serum and spiked saliva samples.

1. Introduction

One of the major causes of death and disability in the world is diabetes mellitus. Currently there is no cure for diabetes mellitus and it is effectively controlled by regular monitoring of physiological blood glucose levels [1]. Traditional glucose sensors are enzymatic sensors; which utilizes glucose oxidase (GOx) on the electrode surface to oxidise glucose [2]. However challenges such as enzyme purification, intricate immobilization of enzyme and denaturing of enzyme limit the application of enzymatic sensors. Moreover, the need of redox shuttle to be present is the biggest barrier that hinders the sensitivity of this method [3–5]. Direct oxidation of glucose on the electrode surface in the absence of any enzyme (non-enzymatic sensor) is a current topic on interest, as it eliminates all the challenges associated with enzymatic sensors. Nanostructured metal oxides are more suitable for non-enzymatic glucose sensors as they possess good electrocatalytic properties, large surface areas and fast electron transfer [6]. In addition, nanostructured metal oxide materials can also counteract the drawbacks such as surface poisoning and reduction of the electrode [2]. High conductivity and catalytic activity are required for successful non-enzymatic glucose sensors. Various metal oxides such as $NiOH_2$ [7], Co_3O_4 [8], CuO, ZnO, SnO [9] etc. have been the subject of various studies for non-enzymatic glucose sensing applications. Among these, Co_3O_4 is of particular consideration due to its electro-catalytic properties, chemical stability and availability [10]. However, Co_3O_4 has low conductivity which results in a glucose sensor with low sensitivity as reported previously in literature [8,11,12]. Recently we have shown that elemental doping is a rational and effective approach to increase the electronic conductivity of Co_3O_4 [13,14]. Recently, Cu loading on Co_3O_4 support has been shown to increase hydrogen evolution due to the cooperative synergistic effect between Cu and Co_3O_4 [15]. Mehrabadi and co-authors have shown that $CuO_{0.3}CoO_{0.7}$ material showed enhanced gas sensing performance compared to pristine Co_3O_4 [16]. Thus, it is expected that the synergism from the combination of intrinsic and extrinsic Cu doping would be extremely interesting in glucose sensing applications and it is expected to achieve significantly improved performance when compared to pristine Co_3O_4.

Conventional electrode fabrication process for glucose sensing requires two step processing. Firstly, the catalysts are prepared in the form of nanoparticles and secondly it is immobilised on the electrode surface with a binder. The presence of additive material can produce contact resistance and obstruct reaction site as they are insulating and chemically inactive, which decreases the sensors performance [17–20]. Various advanced deposition techniques such as pulsed laser deposition (PLD), plasma sputtering, atomic layer deposition (ALD) have been used to fabricate metal oxide films. However, these techniques are capital investment intensive and requires frequent maintenance [21,22]. For the above-mentioned reasons, solution based process is a rational solution to the problem in the conventional systems.

In this study, we report on the facile solution processed deposition of Cu doped Co_3O_4 and its electrochemical glucose sensing ability. The as prepared Cu doped Co_3O_4 electrode showed high sensitivity,

* Corresponding author.
E-mail address: chowdhurym@cput.ac.za (M. Chowdhury).

https://doi.org/10.1016/j.sbsr.2019.100262
Received 19 November 2018; Received in revised form 4 February 2019; Accepted 7 February 2019

selectivity and stability.

2. Experimental procedure

2.1. Chemicals

Micasol detergent, ethanol (C_2H_5OH), fluorine doped tin oxide glass (FTO, 300 mm × 300 mm × 2 mm, surface resistivity ~7 Ω/sq), Cobalt (II) chloride hexahydrate ($CoCl_2.6H_2O$), sodium oleate ($C_{18}H_{33}NaO_2$), hexane (C_6H_{14}), Toluene (C_7H_8), cupric chloride ($CuCl_2.2H_2O$), glucose, fructose, sucrose, sodium chloride (NaCl), potassium chloride (KCl), acetaminophen ($C_8H_9NO_2$), uric acid ($C_5H_4N_4O_3$), ascorbic acid ($C_6H_8O_6$) and human serum were obtained from Sigma Aldrich South Africa and were used as it is without further purification.

2.2. Fabrication of the Cu doped Co_3O_4 electrode

2.2.1. Synthesis of copper doped Co_3O_4

The electrodes were fabricated in two steps. First, a cobalt oleate complex was synthesised by an ion exchange reaction between $CoCl_2.6H_2O$ and sodium oleate. For a typical synthesis, 40 mmol cobaltous chloride and 120 mmol sodium oleate were placed in a solution of 80 ml ethanol, 60 ml de-ionized water and 140 mL hexane. The solution was heated under reflux at 70 °C for 4 h. After refluxing, the upper organic layer containing cobalt oleate complex was washed 3 times in 30 mL distilled water in a seperatory funnel. The cobalt oleate complex was then placed in a petri dish and left to dry in the oven at 60 °C overnight. The residue was discarded appropriately. To prepare the Cu doped Co_3O_4 electrode, 0.09 g of cobalt oleate was dispersed in 0.5 mL toluene via sonication. Solution of $CuCl_2.2H_2O$ (in ethanol) was added to the cobalt oleate solution. The copper solution was added to the cobalt oleate solution at various volume percentages (98: 2 V/V, 90: 10 V/V, 85: 15 V/V, and 80: 20 V/V). This was done to vary the Cu concentration in the Co_3O_4 to find the optimum ratio of Cu: Co_3O_4 for enhanced electrochemical performance.

2.2.2. Electrode preparation

Rectangular pieces of FTO glasses were cut using a diamond glass cutter in accordance to the measurement of 4 cm length and 1.2 cm breath. The cut FTO glasses were cleaned via sonication by detergent for 10 min and rinsed with distilled water and dried under air. 50 µL of the precursor solution was deposited on the FTO glass by spin coating at 4000 rpm for 60 s. The film was then calcined at 350 °C for 10 min. The spin coating and calcination was repeated for $N = 1$ to 6 times as per the number of layers coated to evaluate the role of film thickness. The electrodes were calcined at 350 °C for 4 h at the final layer required. The pristine Co_3O_4 electrode was made the same as above except the fabrication solution was only cobalt oleate solution ($N = 1$ to $N = 5$).

2.2.3. Electrochemical measurements

All the electrochemical measurements were conducted using an Autolab PGSTAT302N potentiostat with Nova 2.0 software. A three electrode cell, consited of: Ag/AgCl (3 M) reference electrode, graphite rod as counter electrode and Cu:Co_3O_4 deposited FTO as working electrode was used for all electrochemical measurments. A quiescent 0.1 M NaOH solution was used as electrolyte for cyclic voltammetry and chronoamperometry measurements. Chronoamperometry was conducted under stirring and at an applied bias potential of + 0.65 V vs Ag/AgCl (3 M).

2.3. Surface characterization

X-ray diffraction (XRD) was used to identify the cobalt phase present in the as prepared electrode. The XRD patterns were recorded utilizing a PANalytical X'Pert PRO PW3040/60 diffractometer with Fe filtered Cu-Kα (λ = 0.154 nm) monochromated radiation source. Scanning electron microscopy (SEM) and energy dispersive X-ray spectroscopy (EDS) was conducted utilizing a Zeiss Auriga field-emission SEM, operated at 5 kV for imaging and 20 kV for EDS analysis. The EDS data was collected using an Oxford X-Max solid-state silicon drift detector, with an objective aperture of 60 µm and count rates between 60 and 120 s employed for high quality spectra. High resolution transmission electron microscopy (HR-TEM), selected area electron diffraction (SAED) and electron energy loss spectroscopy (EELS) data of the samples were collected using an FEI Tecnai F20 field emission gun TEM operated at 200 kV, equipped with a Gatan GIF-2001 energy filter. EELS was utilized to study the electron energy loss near edge fine structure (ELNEFS) signals of cobalt and oxygen ionization edges. Each spectrum was collected in normal parallel beam, bright-field TEM mode for 5 s. During TEM sample preparation, the sensing material was physically removed from the FTO substrates by scraping using a sharp edged razor blade in the presence of ethanol, thereby forming a concentrated solution; this was followed by ultra-sonication for 5 min. One drop of solution (~30 µl) was then drop casted onto a lacey carbon coated Ni grid (3 mm in diameter, 400 mesh) and completed by drying under a Xenon lamp for a further 5 min. Room temperature Hall effect measurements were conducted using an Ecopia Hall Effect Measurement System (HMS-3000 version 3.5) with 0.55 T magnetic field strength.

3. Results and discussion

3.1. Surface characterization of the modified Co_3O_4 electrode

The morphology and structure of the solution deposited film was evaluated by high resolution SEM and TEM. Fig. 1a & b represent the SEM image of the pristine and Cu doped electrodes, respectively. It can be seen from Fig. 1a that the deposited film of pristine Co_3O_4 is uniformly dispersed on the FTO. No hole or crack is observed from the SEM image, highlighting the consistency of the film thickness through the entire geometrical area. However, Cu doped Co_3O_4 film shows bigger nucleation sites through the entire film (Fig. 1b). The increased surface roughness is beneficial for electrochemical activities due to increased surface area [8]. The average film thickness on the Cu doped electrode is 1697 nm (Fig. 1c) and for the pristine electrode, the average film thickness is 357 nm (data not shown). This suggests successful incorporation of Cu into Co_3O_4 host lattice. TEM images of the Cu doped Co_3O_4 are presented in Fig. 1 (d & e). A uniform distribution of Cu was found (Fig. 1 f-h) from elemental X-ray mapping. Quantified EDS data (See supplementary data, Fig. S1) show that the Co and Cu X-ray signals are more or less one-to-one; this explains the relative uniform density of the colour maps for the respective elements.

Fig. 2 a & b represents the SAED patterns of the pristine and Cu doped Co_3O_4 electrode. The first four diffraction rings (Fig. 2a) are identified as that from the face centred cubic (fcc) Co_3O_4 crystal structure yielding $d_{111} = 0.474$ nm, $d_{220} = 0.291$ nm, $d_{311} = 0.249$ nm and $d_{400} = 0.205$ nm, respectively. From these values an average lattice constant of $a = 0.822 \pm 0.003$ nm was determined. Correspondingly, the Cu doped Co_3O_4 (Fig. 2b) electrode sample also exhibited the fcc crystal structure of Co_3O_4 but with a slight increase in the respective d-spacing to $d_{111} = 0.475$ nm, $d_{220} = 0.293$ nm, $d_{311} = 0.250$ nm and $d_{400} = 0.206$ nm. Due to this, there is a small expansion of the average lattice constant compared to the pristine Co_3O_4 sample, $a = 0.826 \pm 0.003$ nm. It can be observed from the XRD pattern (Fig. 2c) that the film contains the Co_3O_4 structure; regardless to the Cu doping. However, a slight increase in full-width-half-maxima can be observed for the Cu doped Co_3O_4 material. This phenomenon indicates strain in the Co_3O_4 matrix due to the successful addition of elemental Cu ions into the Co_3O_4 lattice. Also, the presence of (220), (311) and (400) peaks complements the observation from the TEM and SAED analysis.Fig. 3 compares the ELNEFS data of the Co $L_{3,2}$ ionization edge of the pristine (black curve) and Cu:Co_3O_4 (red curve) samples. Both

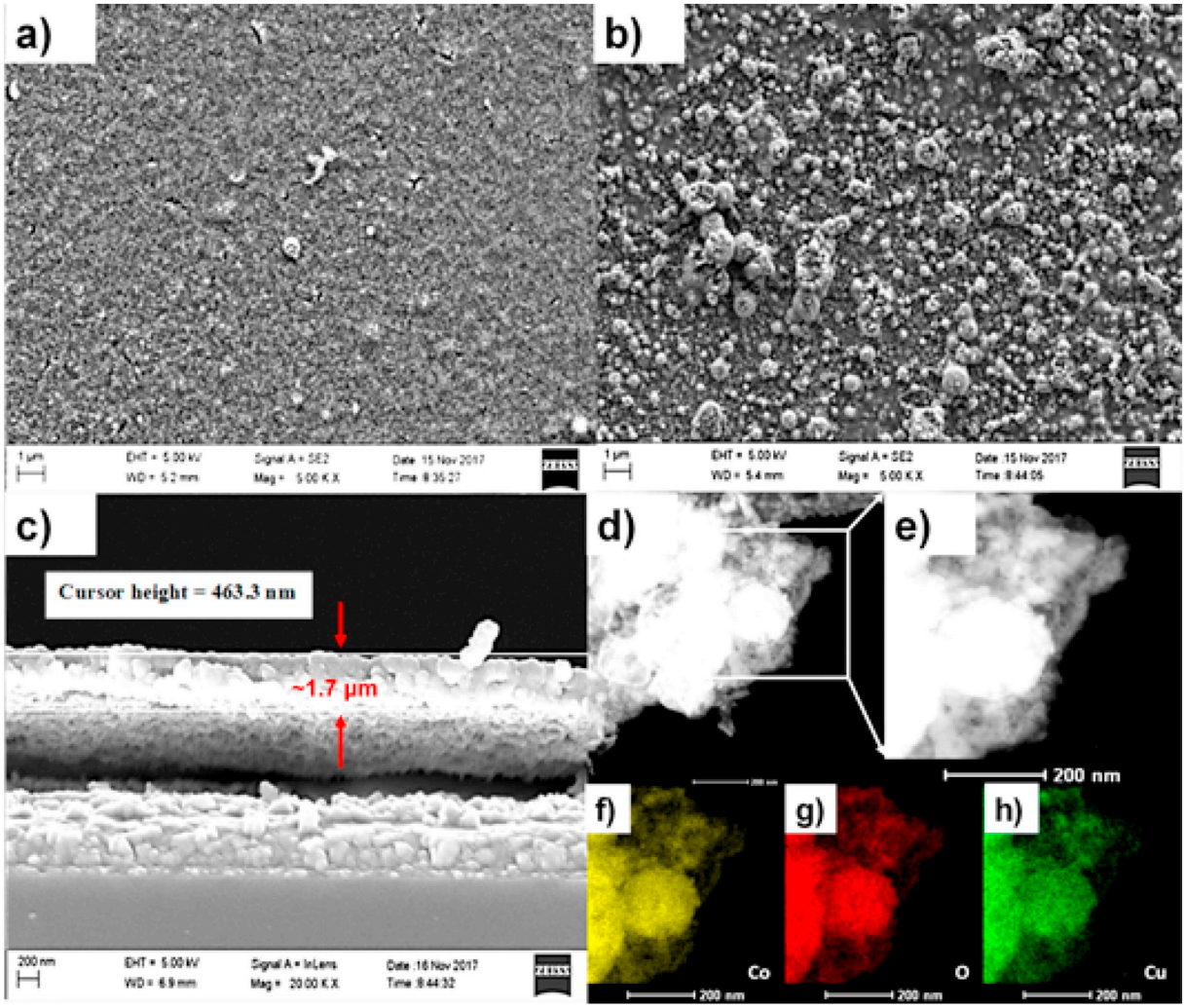

Fig. 1. SEM images of the film surface of pristine (a) Co_3O_4 and (b) Cu doped Co_3O_4; (c) cross sectional view of the Cu doped Co_3O_4 thin film; (d – h) TEM image and X-ray elemental distribution map of the Cu doped Co_3O_4 film.

materials show two sharp peaks at 783 (L_3) and 798 eV (L_2), which correspond to the Co $2p_{3/2}$ and Co $2p_{1/2}$ spin–orbit peaks of the Co_3O_4 spinel [23], respectively. In addition, it can be seen that the characteristic Cu $L_{3,2}$ edge at 931 eV is absent in the Cu:Co_3O_4 specimen, indicating that the Cu as identified in the X-ray elemental maps of Fig. 1, do not exist in either oxide or metallic form in the hybrid material. Rather, at closer inspection of the L_3/L_2 of the Co $L_{3,2}$, widely considered a fingerprint method for determining the Co valence state [23–26], a clearer understanding of the effect of the incorporation of the Cu in the Co_3O_4 matrix is developed. From Fig. 3 an L_3/L_2 ratio of 2.49 and 3.89 is determined for the pristine Co_3O_4 and Cu:Co_3O_4, respectively. The EELS spectra were normalised to the most intense ionization edge in order to compare the changes in the L_3/L_2 ratios in Fig. 3. To show this more clearly, two spectra have been added in the supplementary section (Fig. S2 and Fig. S3). In Fig. S2 it can be seen that the most intense (i.e. L_3) of the pure Co_3O_4 sample peaks at 783.4 eV with an electron count rate of 8051.48, whereas the L_2 edge peaks at 798 eV with a count of 3227.87. As such, an L_3/L_2 ratio for the pure Co_3O_4 sample of 8051.48/3227.87 = 2.494 is obtained. Similarly when doing the background subtraction of the raw Cu:Co_3O_4 spectrum (Fig. S3), an L_3/L_2 = 8617.400/2245.67 = 3.837 is obtained. The ratio of 2.49 is typical for cobalt oxides exhibiting cobalt ions in two oxidation states: one-third of the Co atoms being Co^{2+} in a tetrahedral coordination to oxygen and two thirds Co^{3+} in an octahedral oxygen environment [23,24]. The increase in the L_3/L_2 ratio for the Cu modified Co_3O_4 proves that a change in the $1/3Co^{2+}$ + $2/3Co^{3+}$ coordination occurred upon incorporation of the Cu ions in the Co_3O_4 matrix. The value of 3.89 is typical of pure Co^{2+} and in some instances Co^{4+} valence states [25,26]. However, considering the expansion in lattice parameter measured from the SAED results of Fig. 2 and the distribution of the Cu elements in the X-ray maps of Fig. 1, the increase in L_3/L_2 ratio, and subsequent change in valence state of the Co oxide, is attributed to doping by the Cu atoms.

3.2. Electrochemical behaviour of the Cu doped Co_3O_4 electrodes

Cyclic voltammetry (CV) was utilized to evaluate the performance of the Co_3O_4:Cu electrode for electrocatalytic oxidation of glucose in an alkaline solution of 0.1 M NaOH. Cyclic voltammetry was performed in the potential range between −0.2 V to 0.8 V vs. Ag/AgCl. Various ratios of Cu (98:2; 90:10; 85:15 and 80: 20; Co_3O_4:Cu) was introduced into the Co_3O_4 host lattice structure to find the optimum level of Cu doping for enhanced electrochemical activity. The 90:10 ratio of Co_3O_4:Cu depicted the highest electrochemical activity (current density response) in comparison to the other ratios studied (Fig. S4, supplementary document). Electrode film thickness plays a big role in enhanced electrochemical performance of any sensor. In this study, the electrode film thickness was controlled by increasing the no. of layers deposited (N = 1 to 6) on the FTO substrate. From the EIS study it was found that the resistance for charge transfer (R_{ct}) in 4 layer deposited electrode

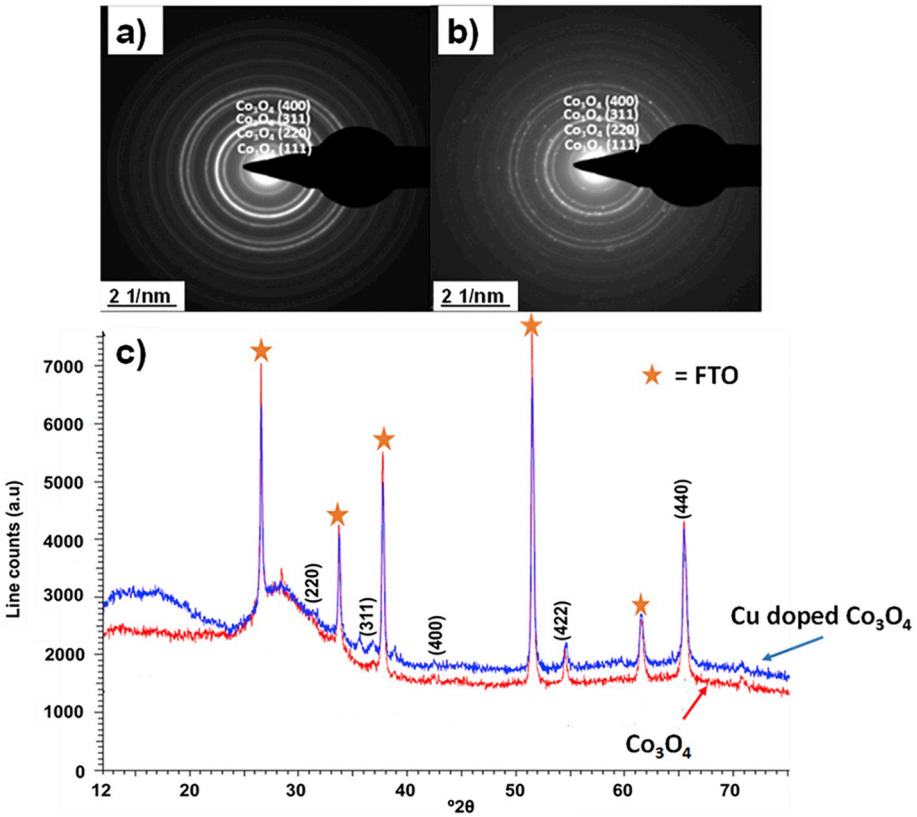

Fig. 2. (a) & (b) Selected area electron diffraction patterns for pristine and Cu doped Co_3O_4 electrode respectively, (c) XRD patterns of the pristine and Cu doped Co_3O_4 electrodes.

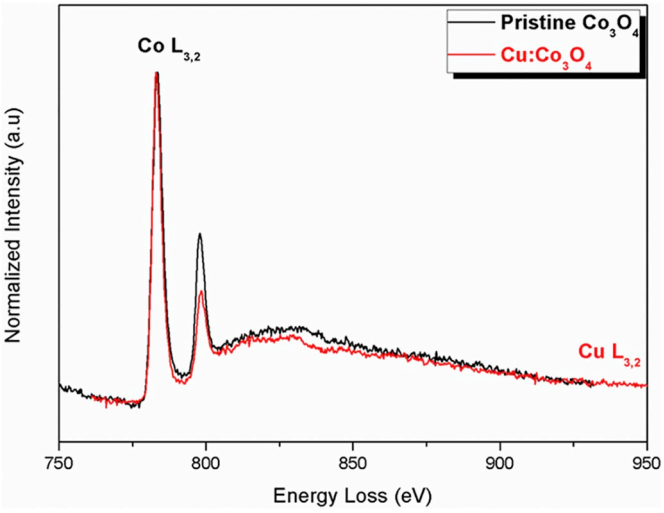

Fig. 3. Electron energy loss spectroscopy results comparing the Co $L_{3,2}$ ionization edge of the pristine Co_3O_4 sample to that of the Cu incorporated Co_3O_4 material.

was significantly lower (data not shown) than the other layers studied. Hence, the 4 layer deposited electrode showed the highest electrochemical activity (Fig. S5, supplementary document). All electrochemical results reported in this study were obtained using a 90:10 ratio of Co_3O_4:Cu with $N = 4$ electrode unless otherwise stated. A comparison between the CV of pristine Co_3O_4 and Cu doped Co_3O_4 highlighted the effect of Cu doping in Co_3O_4 host lattice structure, as the Cu doped Co_3O_4 showed enhanced electrochemical activity compared to pristine Co_3O_4 (Fig. S6, supplementary document). The pristine Co_3O_4 and Cu doped Co_3O_4 electrode exhibited a current density around 2.85 and 3.78 mA/cm^2 respectively in the presence of 5 mM glucose at +0,65 V. The presence of Cu doping in Co_3O_4 enhanced the catalytic oxidation current by 33%. It can be seen from Fig. 4a that there is a significant increase in the anodic current in the presence of 2 mM glucose compared to the absence of glucose. This highlights the glucose sensing ability of the as prepared electrode. Two pairs of redox peaks can be observed (Fig. 4a) due to the electrochemical redox reaction between Co_3O_4 and the OH^- ions [27]. The first pair of redox peaks (I/II) appeared in the relative low potential zone between +0.1 V to +0.3 V, and can be ascribed to the reversible transition between Co_3O_4 and CoOOH. The other set of redox peaks (III/IV) observed in the potential range of +0.6 to 0.7 V can be assigned to the conversion of CoOOH to Co_3O_4 [28]. Interestingly it can be observed from Fig. 4b that with increase in glucose concentration the anodic peak shifts towards more positive potential. The changes in CoO_2 and CoOOH species concentration result in the slight shift of the positive peak. The glucose oxidation mechanism can be summarized as follows:

$$Co_3O_4 + OH^- + H_2O \leftrightarrow 3CoOOH + e^- \quad (1)$$

$$CoOOH + OH^- \leftrightarrow CoO_2 + +H_2O + e^- \quad (2)$$

$$2CoO_2 + C_6H_{12}O_6 \rightarrow 2CoOOH + C_6H_{10}O_6 \quad (3)$$

The change in anodic and cathodic peak current at various scan rate is presented in Fig. 4c. A linear correlation exists between the peaks and the scan rate. This provides evidence of a fast electrochemical process and that the process is a surface controlled process of redox reaction [27].

The interfacial properties of the pristine Co_3O_4 and the modified Co_3O_4:Cu electrode were studied by electrochemical impedance spectroscopy (EIS) and presented in the form of Nyquist plot (Fig. 4d). The Nyquist diagrams did not exhibit a clear semicircle for both the pristine Co_3O_4 and Cu:Co_3O_4 electrodes. Exhibited semicircle and linear part at high and low frequency region can be attributed to charge transfer (R_{ct})

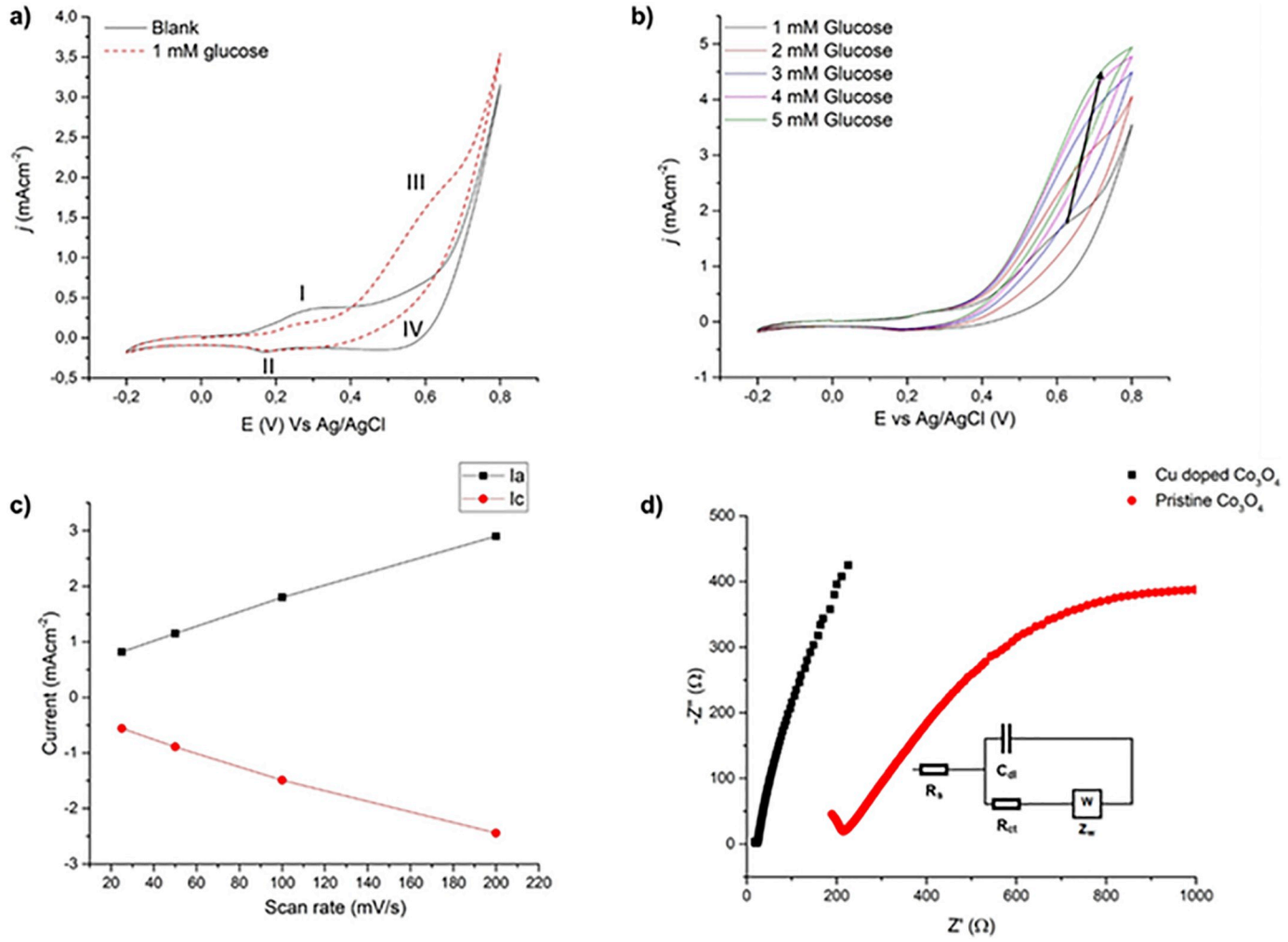

Fig. 4. Electrochemical behaviour of the Cu:Co_3O_4 thin film electrode in 0.1 M NaOH electrolyte solution; a) cyclic voltammogram of the pristine and Cu doped Co_3O_4 in the absence and presence of glucose at a scan rate of 25 mVs^{-1}, b) cyclic voltammetry of the Cu:Co_3O_4 thin film electrode in the presence of various glucose concentration at a scan rate of 25 mVs^{-1}, c) effect of scan rate on the electrochemical behaviour of Cu doped Co_3O_4 thin film electrode and d) Nyquist plot of pristine and Cu doped electrode.

and Warburg impedance (Z_w) respectively which provides indication of the electron transfer kinetics. It can be seen from Fig. 4d that the Cu:Co_3O_4 doped electrode exhibits a smaller semi-circle compared to the pristine electrode, highlighting higher electron transfer kinetics. Randle circuit (inset Fig. 4d) was used to calculate the R_{ct} values for both pristine (R_{ct} = 292 Ω) and Cu doped Co_3O_4 electrode (R_{ct} = 1.09 Ω). The Bode plot presented in supplementary document (Fig. S7) also shows that the charge transfer resistance decrease significantly with the presence of Cu in the Co_3O_4; highlighting the good electrochemical activity of the Cu doped $C_{o3}O_4$. Hall effect measurements were carried out to further evaluate the role of Cu doping in Co_3O_4 host lattice structure. The pristine Co_3O_4 sample was not very conductive, hence the input current was very low i.e. 0.2 μA. The Cu doped sample on the other hand displayed a greater conductivity thus the input current for conductivity measurement was in the range of 25–150 μA. The conductivity increased by three orders of magnitude with the addition of the Cu in Co_3O_4 and found to be 80 and 3.72×10^{-2} /Ωcm for Cu:Co_3O_4 and Co_3O_4, respectively. The increased conductivity is due to the successful Cu-doping of the Co_3O_4, as evinced by the increased carrier (electron) concentration from 1.69×10^{16} /cm^3 (for the pristine Co_3O_4) to 2.95×10^{19} /cm^3 (for the Cu: Co_3O_4). It should be noted that both films exhibited the n-type semiconductor behaviour of the electrodes.

3.3. Chronoamperometry study of the Cu doped Co_3O_4 electrodes

It was shown earlier (Fig. 4 a & b) that the oxidation peak of glucose was in the potential range of 0.6–0.7 V vs Ag/AgCl. Chronoamperometric (CA) detection of glucose was carried out (Fig. 5a) in the potential range of 0.6–0.8 V vs Ag/AgCl to evaluate the role of applied potential on the sensor sensitivity. Chronoamperometric measurement was performed under stirring at a successive addition interval of 30s. The sensor displayed a classical step style increase in current density after each successive addition of glucose at all applied potentials. The response time of the sensor in all cases were < 10 s. From the dose response curve presented in Fig. 5b it was observed that the sensor exhibits two distinctive linear ranges (18.3 μM to 1.44 mM and 1.44–7.36 mM). The sensitivity value was found to be larger in the low concentration range (18.3 μM - 1.44 mM) compared to higher concentration range (1.44–7.36 mM) for all applied potentials (table, inset Fig. 5b). The maximum sensitivity value was calculated to be 1850.4 $\mu Acm^{-2} mM^{-1}$ at +0.6 V (low range). However, the sensitivity in the second linear range increased with increasing applied potential. The reported sensitivity in this study was significantly higher compared to our previous studies [13,14]. The applied potential can be chosen depending on the application of the sensor. The limit of detection (LOD) was calculated utilizing the following equation.

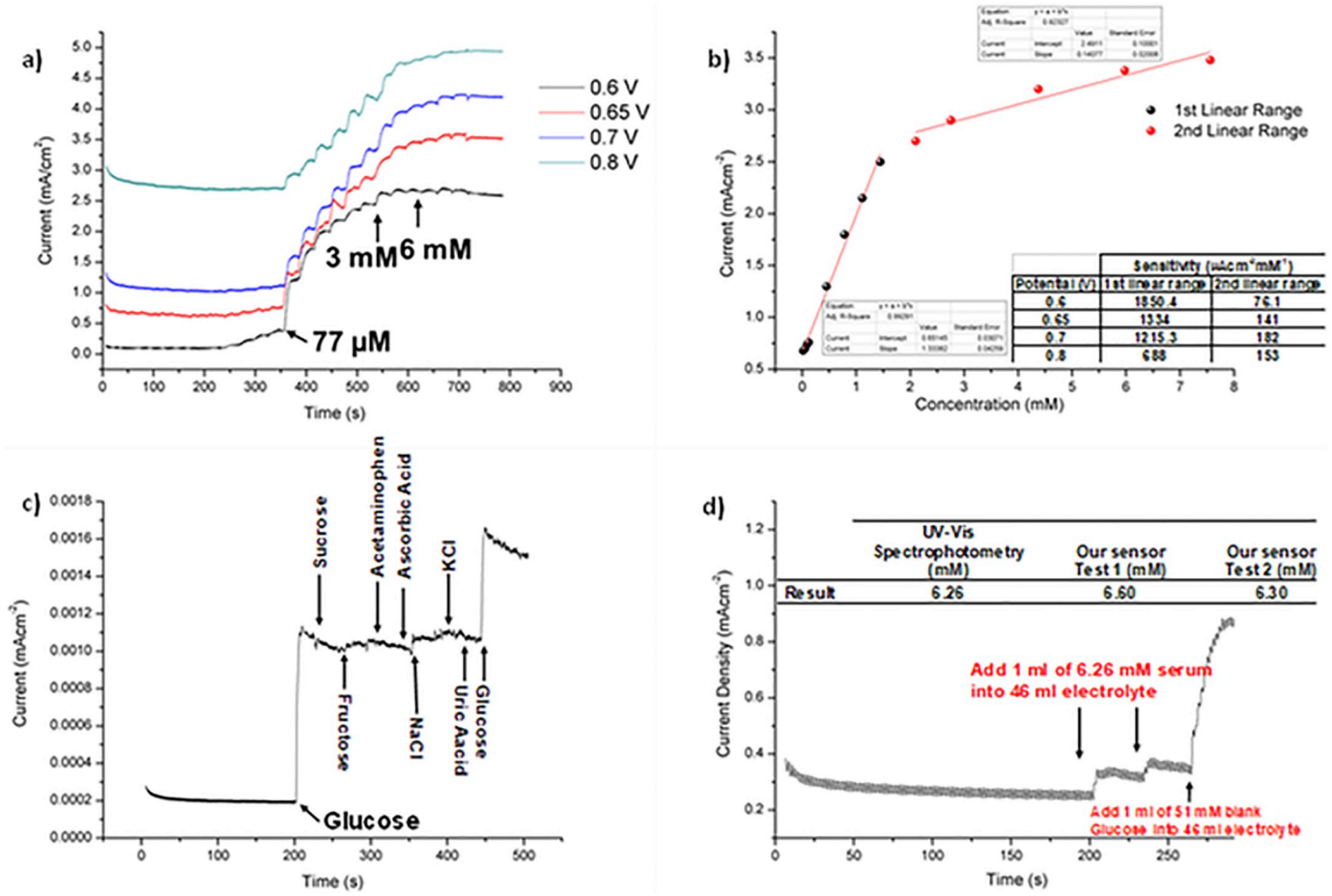

Fig. 5. a) Chrono amperometry of the electrode at different applied potential, b) typical dose response curve generated from CA at +0.65 V, c) Selectivity study of the as prepared electrode and d) comparison of sensor data with conventional glucose detection technique.

$$\mathrm{LOD} = \frac{3\sigma}{\mathrm{m}} \tag{4}$$

σ is the standard deviation of the sample linear range obtained after the addition of the glucose; m is the slope of the calibration curve. The extrapolated LOD was calculated to be 0.153 uM (S/N = 3). Table 1 shows a comparison of the applied potential of several typical non-enzymatic glucose electrodes. Compared with other studies, the present work exhibited high sensitivity and low detection limit with reasonable response time. Interference study (Fig. 5c) was conducted to evaluate the selectivity of the sensor in glucose detection due to the fact that the human blood contains other key species i.e. ascorbic acid (AA), acetaminophen (AC), uric acid (UA), fructose, sucrose, sodium chloride (NaCl) and potassium chloride (KCl). Interference study was conducted using a 1 mM glucose, 0.1 mM fructose, 0.1 mM sucrose, 0.1 mM AA, 0.1 mM AC, 100 mM NaCl and 100 mM KCl solutions respectively at an applied potential of +0.65 V. It can be seen that the sensors' response to glucose is significantly higher than other interference species. Electrode poisoning due to the presence of NaCl and KCl is a common phenomenon in the case of noble metal based sensors. The as developed sensor maintained good response when glucose was added after the successive addition NaCl and KCl and also other interference species. This proves that the developed sensor can be used for reliable measurement of

Table 1
Comparison of glucose detection performance of Cu:Co_3O_4 with other non-enzymatic sensors.

Material	Sensitivity ($\mu A cm^{-2} mM^{-1}$)	Response time (s)	LOD (µM)	Linear range	References
Co_3O_4: TiO_2	2008.82	≤ 5	0.34 µM	3 mM	[27]
Co_3O_4 nano-fibers	36.25	≤ 7	0.97 µM	–	[29]
Co_3O_4/PbO_2	460	≤ 2	0.31 µM	5 uM-1.2 mM	[30]
Co_3O_4-$Ni(OH)_2$	1.089	≤ 5	1.08 u µM	5 uM-40 uM	[31]
Sn: Co_3O_4	921/265	≤ 4	0.10 µM	2 uM-0.5 mM & 0.6 mM–5.5 mM	[14]
Zn: Co_3O_4	193	≤ 7	2.0 µM	5.5 mM–0.62 mM	[13]
Cu_2O-Cu	1620	–	49.0 µM	0–6 mM	[32]
Cu-Cu_2O nanoporous nanoparticles	123.8	–	0.05 µM	0.01–5.5 mM	[33]
Graphene wrapped Cu_2O nanotubes	285	≤ 9	0.003 µM	0.3–3.3 mM	[34]
Co_3O_4/GC	520.7	≤ 6	0.13 µM	< 2 mM	[35]
Cu: Co_3O_4	1850/76 1333/ 141	≤ 10	0.153 µM	18.3 µM-1.44 mM & 1.44 mM–7.6 mM	This work

Table 2
Detection of glucose in saliva sample ($n = 3$).

Spiked (mM)	Measured by Sensor (mM)	% Recovery
0.311	0.32	102
0.615	0.58	94.3
1.678	1.55	92.39

glucose in physiological samples. The good selectivity of the Cu:Co_3O_4 sensor towards glucose at +0.65 V can be attributed to the repelling effect at the Cu:Co_3O_4 surface as was first proposed by Ding and co-authors [8]. The results obtained from the interference study confirm that the developed method for electrode fabrication is suitable for making biosensors for glucose detection. The developed sensor was also applied to detect glucose in human serum sample. Fig. 5d exhibits the chrono amperometric response of the proposed sensor after successive addition of 1 mL serum (6.26 mM glucose concentration) in 46 mL of electrolyte solution. Clear increase in current response was observed after addition of human serum. The concentration of glucose in serum was measured by UV–vis spectrophotometry. The good agreement (Fig. 5d inset) between our proposed sensor and UV–vis spectrophotometry technique highlights the potential application of the non-enzymatic glucose sensor. In order to develop a non-invasive route for glucose detection, the sensor was used to detect glucose in spiked human saliva as a proof of concept. The saliva samples were spiked with different amount of known glucose concentration for electrochemical analysis. Table 2 shows that the obtained recovery is in the range of 92–97%. This highlights the sensor's potential application in glucose detection of real samples.

3.4. Reproducibility, repeatability, stability and shelf life of the proposed sensor

Reproducibility of glucose sensors is vital for the accurate measurement of analyte concentrations. Four individual electrodes were prepared accordingly and tested with 1 mM glucose at 25 mV/s. The anodic oxidation current peaks were then compared for inter electrode reproducibility. The percentage relative standard deviation (% R.S.D) was calculated to be 9% for four sensors. Repeatability tests were performed by measuring the current response of the electrode in 1 mM glucose solution ($n = 5$). Before each measurement, the sensor wash washed with distilled water and dried under air flow to be tested in freshly prepared 1 mM glucose solution immediately. The % R.S.D. was calculated to be 10% between five repeats of the same electrode (Supplementary document, Fig. S8). Chemical stability of the sensor was determined by cyclic voltammetry for 100 cycles (Supplementary document, Fig. S8) in a 1 mM glucose solution at a scan rate of 25 mV/s. It can be seen that no new redox pairs were found even though the anodic current decreases slightly. Hence it can be concluded that the chemical stability of the sensor is good. The shelf life of the sensor was evaluated over a four-week period. The sensor was tested, washed with distilled water and stored under ambient conditions after testing each week. The sensor maintained 80% of the initial current response after the four-week period (data not shown). This highlights the long term storage and testing ability of the proposed sensor.

4. Conclusion

In this study, elemental Cu was successfully substituted into the lattice structure of Co_3O_4 by a chemical solution method. Introduction of Cu resulted in increased electrical conductivity, charge career density and decreased charge transfer resistance in Co_3O_4. This ultimately resulted in enhanced electrochemical activity when compared to pristine Co_3O_4. The as developed Cu doped Co_3O_4 sensor, showed very high sensitivity of 1850 $\mu Acm^{-2} Mm^{-1}$ with a limit detection of 0.153 μM and, was used successfully to measure glucose concentration in human serum and spiked saliva sample.

Acknowledgments

Mahabubur Chowdhury would like to thank the National Research Foundation of South Africa for financial assistance (Grant no: 88220).

Conflicts of interest

The author declares no conflicts of interest.

Appendix A. Supplementary data

Supplementary data to this article can be found online at https://doi.org/10.1016/j.sbsr.2019.100262.

References

[1] J. Luo, H. Zhang, S. Jiang, J. Jiang, X. Liu, Facile one-step electrochemical fabrication of a non-enzymatic glucose-selective glassy carbon electrode modified with copper nanoparticles and graphene, Microchim. Acta 177 (2012) 485–490.
[2] P. Si, Y. Huang, T. Wanga, J. Ma, Nanomaterials for electrochemical non-enzymatic glucose biosensors, RSC Adv. (2012).
[3] J. Li, Y. Li, Y. Zhang, G. Wei, Highly sensitive molecularly imprinted electrochemical sensor based on the double amplification by an inorganic Prussian blue catalytic polymer and the enzymatic effect of glucose oxidase, Anal. Chem. 84 (2012) 1888–1893.
[4] C. Chen, Q. Xie, D. Yang, H. Xiao, Y. Fu, Y. Tan, S. Yao, Recent advances in electrochemical glucose biosensors: a review, RSC Adv. 3 (2013) 4473–4491.
[5] Z. Li, Y. Xin, Z. Zhang, H. Wu, P. Wang, Rational design of binder-free noble metal/metal oxide arrays with nanocauliflower structure for wide linear range nonenzymatic glucose detection, Sci. Rep. 5 (2015) 10617.
[6] C. Zhu, G. Yang, H. Li, D. Du, Y. Lin, Electrochemical sensors and biosensors based on nanomaterials and nanostructures, Anal. Chem. 87 (2014) 230–249.
[7] C.-Y. Ko, J.-H. Huang, S. Raina, W.P. Kang, A high performance non-enzymatic glucose sensor based on nickel hydroxide modified nitrogen-incorporated nanodiamonds, Analyst 138 (2013) 3201–3208.
[8] Y. Ding, Y. Wang, L. Su, M. Bellagamba, H. Zhang, Y. Lei, Electrospun Co3O4 nanofibers for sensitive and selective glucose detection, Biosens. Bioelectron. 26 (2010) 542–548.
[9] S.N.A. Mohd Yazid, I. Md Isa, S. Abu Bakar, N. Hashim, S. Ab Ghani, A review of glucose biosensors based on graphene/metal oxide nanomaterials, Anal. Lett. 47 (2014) 1821–1834.
[10] C.-W. Kung, C.-Y. Lin, Y.-H. Lai, R. Vittal, K.-C. Ho, Cobalt oxide acicular nanorods with high sensitivity for the non-enzymatic detection of glucose, Biosens. Bioelectron. 27 (2011) 125–131.
[11] L.T. Hoa, J.S. Chung, S.H. Hur, A highly sensitive enzyme-free glucose sensor based on Co3O4 nanoflowers and 3D graphene oxide hydrogel fabricated via hydrothermal synthesis, Sensors Actuators B Chem. 223 (2016) 76–82.
[12] T. Liangliang, H. Gege, C. Yanhua, W. Shenping, S. Yongyao, Y. Hengqing, Y. Cong, C. Yanling, L. Lu, Co_3O_4 based non-enzymatic glucose sensor with high sensitivity and reliable stability derived from hollow hierarchical architecture, Nanotechnology 29 (2018) 075502.
[13] M. Chowdhury, F. Cummings, M. Kebede, V. Fester, Binderless solution processed Zn doped Co3O4 film on FTO for rapid and selective non-enzymatic glucose detection, Electroanalysis 29 (2017) 578–586.
[14] M. Chowdhury, C. Ossinga, F. Cummings, J. Chamier, M. Kebede, Novel Sn doped Co3O4 thin film for nonenzymatic glucose bio-sensor and fuel cell, Electroanalysis 29 (2017) 1876–1886.
[15] Y. Yamada, K. Yano, Q. Xu, S. Fukuzumi, Cu/Co3O4 nanoparticles as catalysts for hydrogen evolution from Ammonia borane by hydrolysis, J. Phys. Chem. C 114 (2010) 16456–16462.
[16] Z.S. Mehrabadi, A. Ahmadpour, N. Shahtahmasebi, M.M.B. Mohagheghi, Synthesis and characterization of Cu doped cobalt oxide nanocrystals as methane gas sensors, Phys. Scr. 84 (2011) 015801.
[17] H.S. Jeon, M.S. Jee, H. Kim, S.J. Ahn, Y.J. Hwang, B.K. Min, Simple chemical solution deposition of Co3O4 thin film electrocatalyst for oxygen evolution reaction, ACS Appl. Mater. Interfaces 7 (2015) 24550–24555.
[18] H. Shi, G. Zhao, Water oxidation on spinel NiCo2O4 nanoneedles anode: microstructures, specific surface character, and the enhanced electrocatalytic performance, J. Phys. Chem. C 118 (2014) 25939–25946.
[19] C. Yuan, H.B. Wu, Y. Xie, X.W. Lou, Mixed transition-metal oxides: design, synthesis, and energy-related applications, Angew. Chem. Int. Ed. 53 (2014) 1488–1504.
[20] M. Cabo, E. Pellicer, E. Rossinyol, M. Estrader, A. Lopez-Ortega, J. Nogues, O. Castell, S. Surinach, M.D. Baro, Synthesis of compositionally graded nanocast NiO/NiCo2O4/Co3O4 mesoporous composites with tunable magnetic properties, J. Mater. Chem. 20 (2010) 7021–7028.
[21] M.E. Donders, H.C.M. Knoops, M.C.M. Van, W.M.M. Kessels, P.H.L. Notten, Remote

plasma atomic layer deposition of Co3O4 thin films, Journal of Electrochemical Society 158 (2011) G92–G96.
[22] W. Estrada, M.C.A. Fantini, S.C. de Castro, C.N. Polo da Fonseca, A. Gorenstein, Radio frequency sputtered cobalt oxide coating: structural, optical, and electrochemical characterization, J. Appl. Phys. 74 (1993) 5835–5841.
[23] Z.L. Wang, J.S. Yin, Y.D. Jiang, EELS analysis of cation valence states and oxygen vacancies in magnetic oxides, Micron 31 (2000) 571–580.
[24] H.A.E. Hagelin-Weaver, G.B. Hoflund, D.M. Minahan, G.N. Salaita, Electron energy loss spectroscopic investigation of co metal, CoO, and Co3O4 before and after Ar+ bombardment, Appl. Surf. Sci. 235 (2004) 420–448.
[25] B.M. Abu-Zied, S.M. Bawaked, S.A. Kosa, W. Schwieger, Effect of microwave power on the thermal genesis of Co3O4 nanoparticles from cobalt oxalate micro-rods, Appl. Surf. Sci. 351 (2015) 600–609.
[26] D. Barreca, A. Gasparotto, O.I. Lebedev, C. Maccato, A. Pozza, E. Tondello, S. Turner, G. Van Tendeloo, Controlled vapor-phase synthesis of cobalt oxide nanomaterials with tuned composition and spatial organization, CrystEngComm 12 (2010) 2185–2197.
[27] Z. Gao, L. Zhang, C. Ma, Q. Zhou, Y. Tang, Z. Tu, W. Yang, L. Cui, Y. Li, TiO2 decorated Co3O4 acicular nanotube arrays and its application as a non-enzymatic glucose sensor, Biosens. Bioelectron. 80 (2016) 511–518.
[28] I.G. Casella, M. Gatta, Study of the electrochemical deposition and properties of cobalt oxide species in citrate alkaline solutions, J. Electroanal. Chem. 534 (2002) 31–38.
[29] Y. Ding, Y. Wang, L. Su, M. Bellagamba, H. Zhang, Y. Lei, Electrospun Co3O4 nanofibers for sensitive and selective glucose detection, Biosens. Bioelectron. 26 (2010) 542–548.
[30] X. Chen, G. Wu, Z. Cai, M. Oyama, X. Chen, Advances in enzyme-free electrochemical sensors for hydrogen peroxide, glucose, and uric acid, Microchim. Acta 181 (2013) 689–705.
[31] M. Rahman, A.J.S. Ahammad, J.-H. Jin, S.J. Ahn, J.-J. Lee, A comprehensive review of glucose biosensors based on nanostructured metal-oxides, Sensors 10 (2010) 4855–4886.
[32] G. Wang, X. He, L. Wang, A. Gu, Y. Huang, B. Fang, B. Geng, X. Zhang, Non-enzymatic electrochemical sensing of glucose, Microchim. Acta 180 (2013) 161–186.
[33] Y. Zhao, Y. Li, Z. He, Z. Yan, Facile preparation of Cu–Cu_2O nanoporous nanoparticles as a potential catalyst for non-enzymatic glucose sensing, RSC Adv. 3 (2013) 2178–2181.
[34] J. Luo, S. Jiang, H. Zhang, J. Jiang, X. Liu, A novel non-enzymatic glucose sensor based on Cu nanoparticle modified graphene sheets electrode, Anal. Chim. Acta 709 (2012) 47–53.
[35] C. Hou, Q. Xu, L. Yin, X. Hu, Metal–organic framework templated synthesis of Co3O4 nanoparticles for direct glucose and H2O2 detection, Analyst 137 (2012) 5803–5808.